

Search for narrow resonances in the lepton final state at CMS

G. Kukartsev

Department of Physics and Astronomy, Brown University, Providence, RI, USA

We discuss the results of searches for high-mass narrow resonances decaying into pairs of leptons using pp collisions at 7 TeV delivered by LHC and collected with the CMS detector in 2010 and 2011. These include searches for the $Z^{0'}$ bosons and RS gravitons.

1. Introduction

Several theoretical models predict new TeV-scale resonances decaying into a pair of leptons. Models of particular interest for the presented analysis include the Sequential Standard Model (SSM) with standard-model-like couplings, and certain grand-unification-motivated models (Ψ) [1]. Both predict narrow Z^0 -boson-like states ($Z^{0'}$). We also consider Kaluza-Klein excitations in the Randall-Sundrum (RS) model of extra dimensions (G_{KK}) [2, 3]. We use the four listed models as benchmarks while we search for a narrow resonance, which is similar to the SSM $Z^{0'}$, in the dimuon and the dielectron channels. We perform a likelihood-based shape analysis of the reconstructed dilepton invariant mass (m_{ll}) spectra. The approach provides robustness against uncertainties in the absolute background rate.

The recent searches for $Z^{0'} \rightarrow l^+l^-$ and $G_{KK} \rightarrow l^+l^-$ were published by the Tevatron experiments [4–7]. There are indirect constraints from LEP-II [8–11].

2. Detector and Experiment

CMS is a general-purpose particle detector located at the LHC proton-proton collider at CERN. A prominent feature of the detector is a superconducting solenoid with the internal diameter of 6 m and an axial field of 3.8 T. The solenoid encloses the pixel detector, the silicon tracker, the crystal electromagnetic calorimeter (ECAL) and the brass and scintillator hadron calorimeter (HCAL). Outside the solenoid there is a steel flux return yoke instrumented with the gas ionization detectors, which constitute the CMS muon system. A diagram of the detector is shown in Figure 1. Further details can be found elsewhere [12]. For the presented results, 1.1 fb^{-1} of integrated luminosity were used.

3. Data and Monte Carlo

The presented results were obtained using the data recorded by the CMS experiment in 2011. The data were taken using proton-proton colliding beams with the center-of-mass energy of 7 TeV. The size of the dataset corresponds to an integrated luminosity of approximately 1.1 fb^{-1} . The size of the data sample used in the dielectron analysis is 25 pb^{-1} smaller due to different quality requirements for the data.

The signal and background processes were modeled using Monte Carlo simulations. Depending on the process, PYTHIA v6.424 [13], MADGRAPH [14] and POWHEG v1.1 [15–17] event generators together with the CTEQ6L1 [18] parton distribution function (PDF) set were used. The full CMS detector simulation was done with GEANT4 [19]. The generated events were passed through the CMS trigger simulation and full reconstruction sequence.

4. Event Selection

We developed dedicated selection criteria for each of the two dilepton channels under consideration. Even though the underlying physics processes under study are similar, reconstruction of different lepton flavors in the detector differs substantially. For electrons, we reconstruct the transverse energy using calorimeter information, while the

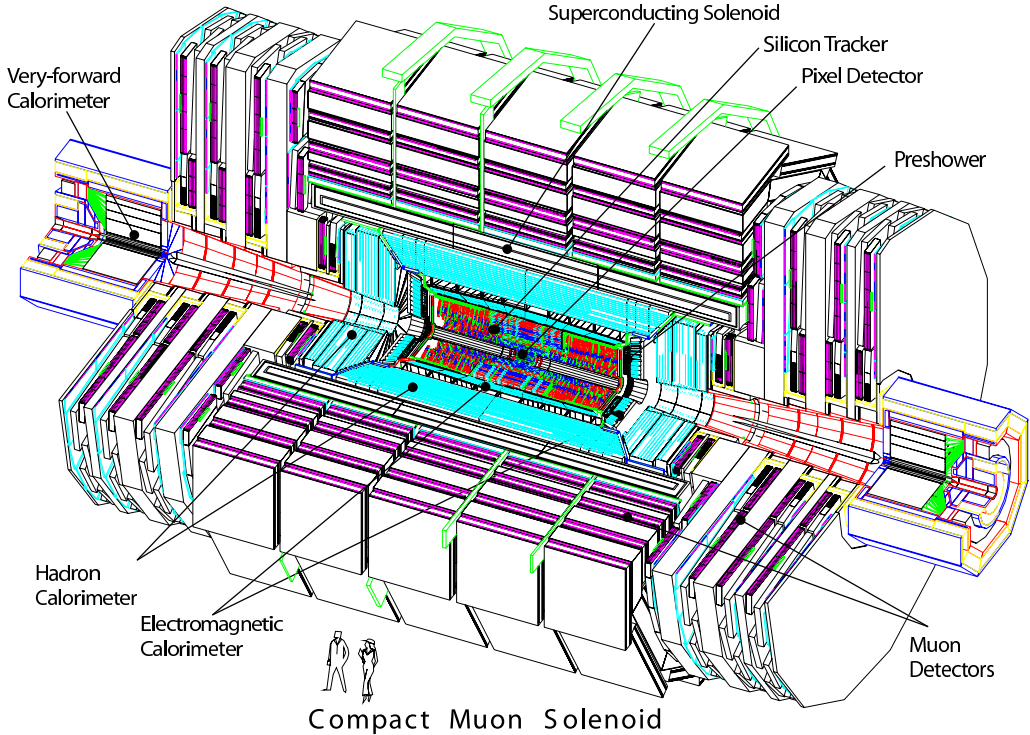


Figure 1: The CMS detector.

muon reconstruction is based on the tracking and the muon systems for the measurement of the transverse momenta. Dilepton invariant mass reconstruction deteriorates for higher values in the dimuon channel and improves in the dielectron channel. We require the muons to be reconstructed with the opposite charge, and do not impose this restriction on dielectron pairs. For the dimuon pairs reconstruction, we reduce systematic uncertainty by performing data-driven studies with cosmic-ray muons. The dielectron channel entails higher background rates from misreconstructed strong scattering signal, and requires tighter selection, which leads to lower efficiency and acceptance.

4.1. Trigger

For the dimuon pair event candidates, we used a single muon trigger with sufficiently high minimum transverse momentum requirement ($p_T > 30$ GeV). The muon was firstly required to be detected in the muon system, and then matched to a track in the silicon tracker. For dielectron pairs, the trigger requires two sufficiently energetic deposits (33 GeV) in ECAL, with at least one of the deposits matched to level-one deposit. The corresponding deposit in HCAL must be small (less than 15%). In later portions of the dataset, a match to the activity in the silicon pixel tracker was required.

4.2. Lepton Reconstruction and Pile-up

Standard CMS techniques apply to the reconstruction, calibration and identification of the leptons [20–22]. For all leptons, the reconstructed track was required to be consistent with the beam interaction point, to be topologically isolated from the hadronic signatures, and to be sufficiently energetic in the plane transverse to the beam axis ($p_T > 35$ GeV for muons and electrons in the ECAL barrel, $p_T > 40$ GeV for endcap electrons). The muons are then reconstructed via a global fit of the tracker and the muon system information with proper quality requirements met: there should be enough hits (more than 10) in the silicon tracker, at least 1 hit in the pixel detector, and a

track reconstructed in the tracker and extrapolated to the muon system must be compatible with the hits in the muon system, with hits in at least 2 of the muon stations. The transverse impact parameter relative to the beam interaction point is required to be less than 0.2 cm. The electrons are reconstructed as an ECAL cluster matched to a track in the silicon tracker. The ECAL cluster seeds the track in the pixel detector, which in turn seeds the track in the tracker. Each track must have at least five hits, and a hit in each of the three pixel layers. The reconstructed electron candidate must be within either barrel ($|\eta| < 1.442$) or endcap ($1.56 < \eta < 2.5$) ECAL acceptance regions, and less than 5% of the energy must be deposited in HCAL.

Leptons are required to be isolated from other activity in the tracker, in order to suppress background from jets misreconstructed as leptons, and from non-prompt leptons. The isolation is defined using a cone $\delta R = \sqrt{(\delta\eta)^2 + (\delta\phi)^2}$ centered on the lepton axis where η is pseudo-rapidity and ϕ is the azimuthal angle relative to the beam axis.

For the muon, the sum of transverse momenta of all other tracks, consistent with the primary vertex, in the cone of 0.3 must be less than 10% of the muon p_T . The efficiency of this isolation requirement was shown to be stable with the number of primary vertexes as indication of robustness against pile-up in a higher instantaneous luminosity regime.

For the electron, the sum of all track p_T in the cone of 0.04 is required to be less than 7 GeV in the barrel of ECAL, and less than 15 GeV for the endcap. The tracks are required to be consistent with the reconstructed primary vertex. The calorimeter isolation for the electrons requires that the sum of E_T of all deposits in the ECAL and the HCAL to be less than $0.03E_T + 2$ GeV relative to the the electron E_T . For the electrons in endcap, we exploit the HCAL segmentation along the beam axis. The isolation energy is required to be less than $0.03 \cdot \max(0, E_T - 50 \text{ GeV}) + 2.5 \text{ GeV}$ where E_T is determined from ECAL and the first layer of HCAL. In the second layer, the HCAL E_T must be less than 0.5 GeV. Additionally, the shape of the transverse energy deposit is required to be compatible with the expected electron signal, and a good match in η and ϕ with the corresponding track is required.

4.3. Lepton pair selection

We select events with two reconstructed leptons: either muons or electrons, originating from a well-reconstructed primary vertex. The vertex must be within 2 cm from the beam interaction point in the transverse plane, and within 24 cm along the beam axis, to suppress cosmic ray background. For the muon pair event candidates, an additional protection against cosmic muons is required as an opening angle between the two muons being less than $(\pi - 0.02)$.

For the dimuon events, we require opposite charges for the two muons as it reduces the fraction of events with a large mismeasurement of the momentum. We suppress events with many poorly reconstructed tracks in order to reduce beam background. At least one muon has to match a high-level trigger (HLT) muon. As an additional quality requirement, the muon pair is required to be consistent with a common vertex.

For the electron pair events, at least one of the electrons is required to be reconstructed in the barrel part of the detector. In order to suppress background from photon conversions, we impose requirement on the distance to the nearest track and an opening angle with it.

4.4. Efficiency and Acceptance

We measure efficiency of triggering, lepton reconstruction and identification with “tag-and-probe” method [20, 22]. We use a pure sample of dimuon pairs requiring that their invariant mass is consistent with the Z boson mass ($60 \text{ GeV} < m_{11} < 120 \text{ GeV}$). One of the muons in the pair is reconstructed with stringent quality requirements (tag), and the other is used as a probe for efficiency estimates. Contributing factors also include track reconstruction and electron clustering. We measure the single muon trigger efficiency to be $95.0\% \pm 0.3\%$ in the barrel and $89.9\% \pm 0.4\%$ in the endcap. The efficiency of the muon identification is measured to be $96.4\% \pm 0.2\%$ in the barrel and $96.0\% \pm 0.3\%$ in the endcap. The efficiency of the track reconstruction in the internal tracker is found to be above 99% in the whole acceptance range. Figure 2 represents the overall acceptance and efficiency values for the dielectron channel, as a function of the dilepton invariant mass. Similar behavior with higher overall acceptance and efficiency values is observed in the dimuon channel.

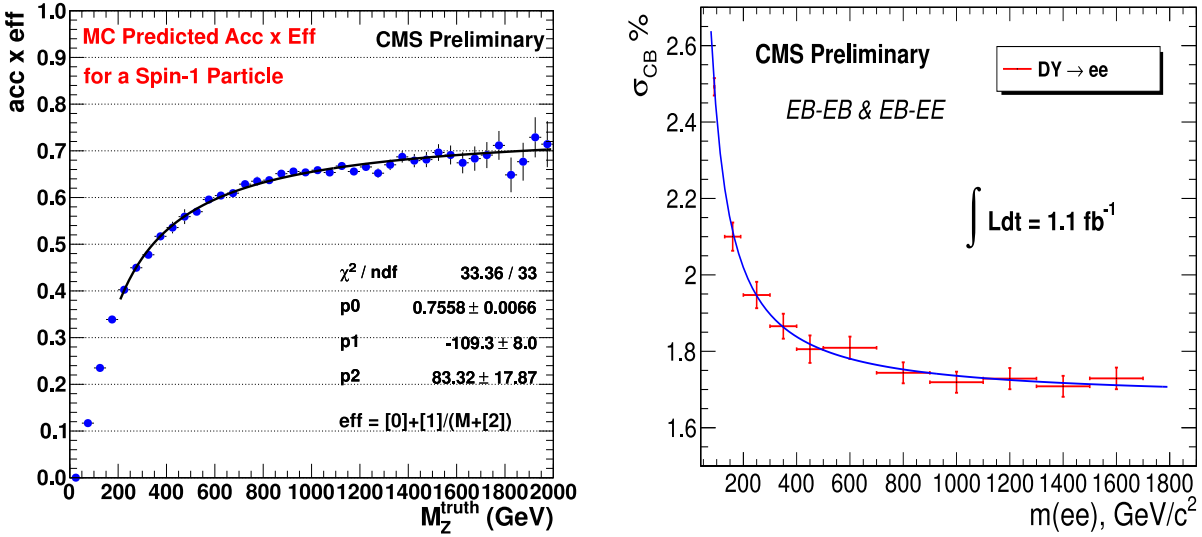


Figure 2: Acceptance and efficiency (left) and invariant mass resolution (right), dielectron channel.

5. Resolution

We study detector performance using Standard Model processes with W and Z mesons and their leptonic final states. We also use cosmic muons. The muon momentum resolution ranges from 1% at few tens of GeV (Z boson peak scale) to approximately 10% above 1 TeV. Tracker-based reconstruction yields better performance at low momenta, while the muons reconstructed in the muon system have better resolution at high momenta. However, energy loss in the steel yoke and showers in the muon chambers can spoil the global fit. We find that adding muon system hits to the tracker-based fit improves resolution for muons with p_T greater than approximately 200 GeV [23]. The most comprehensive algorithm ("Tune P") makes track-by-track decisions about which hits in which subsystems to use. The resolution is also sensitive to the alignment of the muon and the tracker systems.

Unlike for muons, the electron energy resolution improves with energy. The ECAL resolution is better than 0.5% for unconverted photons with transverse energies above 100 GeV. The invariant mass resolution of dielectron pairs is modeled with a Crystal Ball function and obtained from Monte Carlo simulation, with additional smearing applied. The smearing is obtained from comparisons of the Z -boson peak fits in data and Monte Carlo simulation of the $Z \rightarrow ee$ process. At 1 TeV, the dielectron invariant mass resolution is approximately 1.3% when both electrons are in the barrel acceptance region, and approximately 2.4% when one of the electrons is in the endcap region. For the electrons in the barrel section of the detector, energy scale is established using neutral pions and checked using the Z peak.

6. Background

The Drell-Yan process produces the dominant irreducible background, with the next biggest contribution from the top pair and other top-like processes (tW , diboson and $Z \rightarrow \tau\tau$). The remaining background comes from jet misidentification as leptons (1% – 5% depending on the channel), and from cosmic muons in the dimuon channel. We found that the contribution from the latter, and from diphoton processes misreconstructed as dielectrons are negligible. Figures 3 and 4 depict the observed dilepton data overlaid with the background components. The individual components are normalized to next-to-leading order, and then to the Z -boson peak in data. The overall background rate and the shape of the dilepton invariant mass distribution are taken from the Drell-Yan Monte Carlo corrected to next-to-next-to-leading-order with **FEWZz v1.X** [24], **PYTHIA v6.409** and **CTEQ6.1 PDF** [25]. For

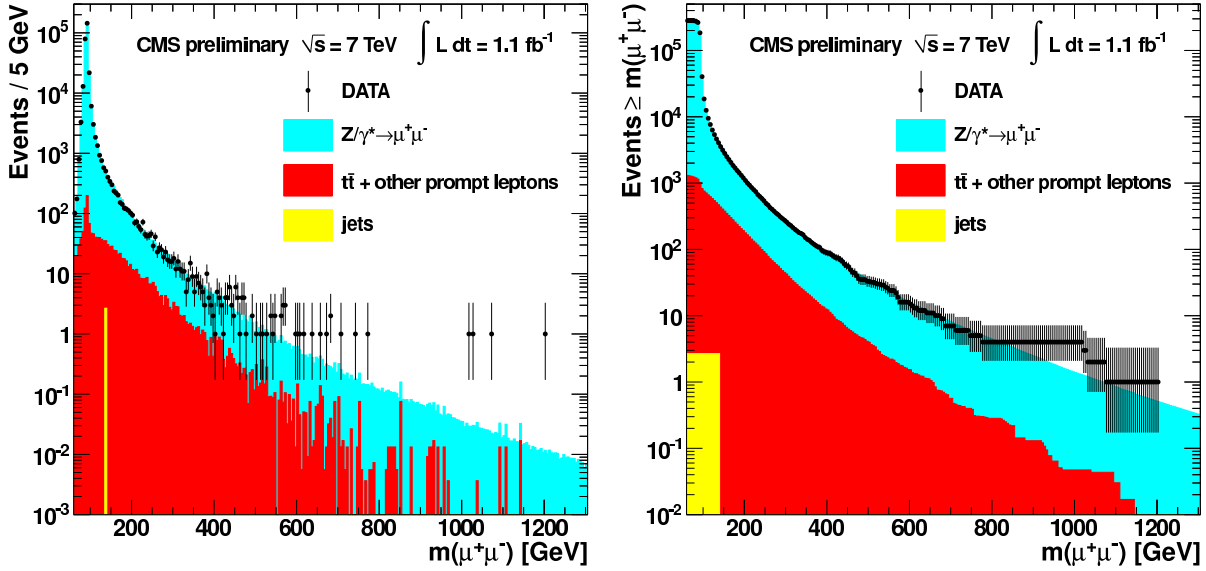


Figure 3: Dimuon invariant mass (left) and the corresponding cumulative spectrum (right). Individual components are normalized to NLO and then together to the Z-boson peak.

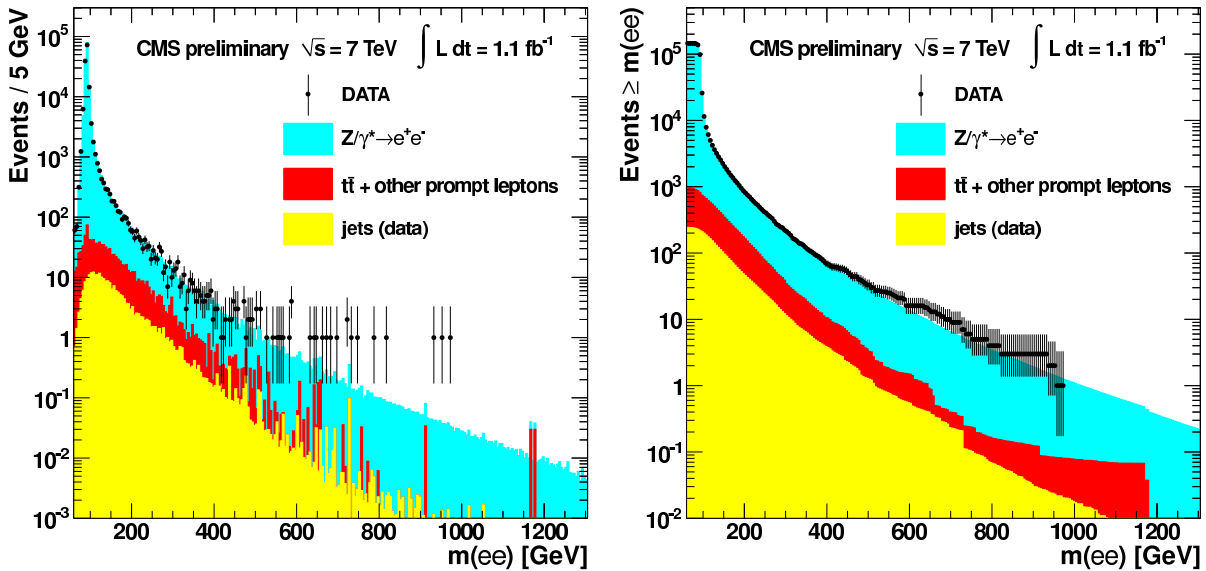


Figure 4: Dielectron invariant mass (left) and the corresponding cumulative spectrum (right). Individual components are normalized to NLO and then together to the Z-boson peak.

the purposes of setting the limits on the dilepton resonance cross section, the variation in the shape due to added top-like and other background sources (5% – 10%), the uncertainties in k-factor, generator choice and PDF sets are covered conservatively by a background rate uncertainty of 20%(15%) in the dimuon (dielectron) channel.

As a cross check of the top-like background model, we compare data and Monte Carlo distributions of the dilepton invariant mass where the flavor and electric charge of the two leptons are required to be different (“ $e\mu$ ” method). The reasoning is that if the two leptons do not originate from a resonance, there is no special reason for them to be of the same flavor. For each dielectron and dimuon event, we expect to observe nearly two $e\mu$ events (the

actual ratio is slightly different due to different efficiencies for electrons and muons). Figure 5 demonstrates the comparison between data and Monte Carlo for the $e\mu$ events, which we find satisfactory.

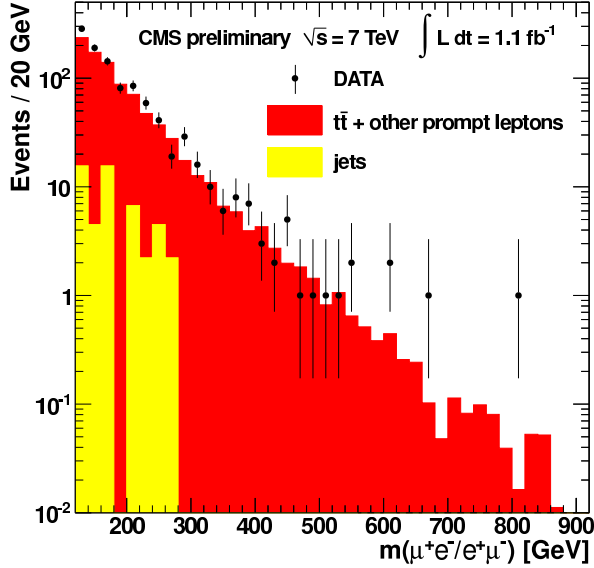


Figure 5: Invariant mass of an electron and a muon of the opposite charge.

7. Statistical Inference

We set 95% C.L. upper limits on the cross section ratio as defined in Equation 5, assuming uniform prior on the parameter of interest and Lognormal likelihood constraint terms on the nuisance parameters in order to model systematic uncertainties. We use the likelihood formalism to estimate the model parameters (via maximum likelihood, ML), and to build a likelihood ratio to be used as a test statistic. In the Bayesian methods the likelihood is further multiplied by priors to obtain the posterior pdf. We define the unbinned likelihood for a data set as

$$L(\mathbf{x}|\boldsymbol{\theta}, \boldsymbol{\nu}) = \prod_{i=1}^N f(x_i|\boldsymbol{\theta}, \boldsymbol{\nu}), \quad (1)$$

where the product is over the events in the data set \mathbf{x} , $f(x|\boldsymbol{\theta}, \boldsymbol{\nu})$ is the probability density function of the observable x , x_i is the value of the observable in the i -th event, $\boldsymbol{\theta}$ is a vector of the model parameters of interest, $\boldsymbol{\nu}$ is a vector of nuisance parameters.

It is often convenient and advantageous to define an extended likelihood by adding the Poisson term. It provides the normalization of the data in terms of the event yield:

$$L(\mathbf{x}|\mu, \boldsymbol{\theta}, \boldsymbol{\nu}) = \frac{\mu^N e^{-\mu}}{N!} \prod_{i=1}^N f(x_i|\boldsymbol{\theta}, \boldsymbol{\nu}), \quad (2)$$

where N is the number of events in the data sample $\{x_i\}$, μ is the Poisson mean number of events. In the following we will use extended likelihoods everywhere.

It is useful to define the profile likelihood ratio test statistic

$$t_{\boldsymbol{\theta}} = -2 \ln \lambda(\boldsymbol{\theta}) = -2 \ln \frac{L_B(\boldsymbol{\theta}, \hat{\boldsymbol{\nu}}_B)}{L_{S+B}(\boldsymbol{\theta}, \hat{\boldsymbol{\nu}}_{SB})}, \quad (3)$$

where L_B and L_{S+B} are the likelihood values for the background-only and for the signal-plus-background models, and ν_B is a subset of ν_{SB} . The *hat* notation ($\hat{\cdot}$) symbolizes the ML estimator, i.e. $\hat{\theta}$ is the value of θ that maximizes the likelihood for a given model. The double hat notation ($\hat{\hat{\cdot}}$) stands for a conditional ML estimator for a given value of a parameter of interest, i.e. $\hat{\nu}$ is the value of ν that maximizes the likelihood for a given model, for a given value of θ .

There are several $Z^{0'}$ models that we consider in the analysis. In the Sequential Standard Model (SSM), the $Z^{0'}$ has the same couplings as the standard model Z boson. The Ψ model is based on an E_6 gauge symmetry. For the models overview see Z-Boson searches in [26]. We use the SSM model by default everywhere unless explicitly stated otherwise.

For the $Z^{0'}$ search, we define the signal-plus-background likelihood as

$$L_{S+B}(\mathbf{m}|\theta, \nu) = \frac{\mu^N e^{-\mu}}{N!} \prod_{i=1}^N \left(\frac{\mu_S(\theta)}{\mu} f_S(m_i|\nu_S) + \frac{\mu_B}{\mu} f_B(m_i|\nu_B) \right), \quad (4)$$

where \mathbf{m} is the dataset in which m_i is the value of the observable m (the invariant mass of the lepton pair) in i -th event, θ denotes the parameter of interest, either the cross section or the cross section ratio, as defined further, ν is the vector of the nuisance parameters, f_S and f_B are the PDFs for the signal and the background (specific shapes are defined later in the document), N is the total number of events observed, μ_S and μ_B are the expected signal and the background event yields, respectively, and $\mu = \mu_S + \mu_B$ is the total number of events expected. Note that the expected signal yield μ_S is a function of the parameter of interest. The parameter of interest is the cross section ratio

$$R_\sigma = \frac{\sigma_{Z^{0'} \rightarrow \ell^+ \ell^-}}{\sigma_{Z^0 \rightarrow \ell^+ \ell^-}}, \quad (5)$$

where $\sigma_{Z^0 \rightarrow \ell^+ \ell^-}$ is the cross section multiplied by the branching ratio for $pp \rightarrow Z^0 \rightarrow \ell^+ \ell^-$. Such an approach allows to exclude the uncertainty on the integrated luminosity from the measurement. In this case, we parameterize the expected signal yield as

$$\mu_S = N_Z \cdot R_\sigma \cdot \frac{\epsilon_{sel}(Z^{0'}) \cdot \mathcal{A}(Z^{0'})}{\epsilon_{sel}(Z^0) \cdot \mathcal{A}(Z)} \equiv N_Z \cdot R_\sigma \cdot R_\epsilon \cdot R_\mathcal{A}. \quad (6)$$

Here N_Z is the observed number of Z^0 events, and $R_\epsilon \cdot R_\mathcal{A}$ denotes the fraction in Equation 6. The PDF, which represents the $Z^{0'}$ signal model, is

$$f_S(m_{ll}|M, \Gamma, w) = \text{BW}(m_{ll}|M, \Gamma) \otimes \text{Gaussian}(0, w), \quad (7)$$

where m_{ll} is the invariant mass of the two leptons (the observable), BW stands for the resonant Breit-Wigner shape, Γ is its width, w is the width of the Gaussian resolution function. For combining multiple analysis channels, the corresponding likelihoods are multiplied together in order to build the combined likelihood.

8. Systematic uncertainty

We combine all systematic uncertainties into three components that we treat independently: an uncertainty on signal sensitivity (includes uncertainties on signal and Z acceptances and efficiencies and on the Z event count), the background rate uncertainty, which is described in Section 6, and the mass scale uncertainty in the dielectron channel (1%).

9. Results

We present reconstructed dilepton invariant mass distributions in the CMS data in Figures 3 and 4 superimposed with the individual background components from Monte Carlo. We use the mass spectra to set 95% C.L. Bayesian

upper limits on the dilepton resonance cross section ratio (Equation 5). We use several popular theoretical models to set lower limits on the corresponding resonance masses, including the Sequential Standard Model $Z^{0'}$. Figure 6 displays the observed limits overlaid with the median expected limits and 1- and 2-standard deviation quantile bands. Theoretical estimates for four popular theoretical models are overlaid as well. Figure 7 displays similar limit plots for the combination of the dimuon and dielectron channels. The likelihood ratio in Equation 3 is asymptotically distributed as a χ^2 distribution with number of degrees of freedom equal to the difference in the numbers of free parameters between the two models.

By combining the two channels, we exclude $Z^{0'}$ masses for the SSM and E6-motivated Ψ model below 1940 GeV and 1620 GeV, respectively. The corresponding limits in the individual dimuon(dielectron) channels are 1780(1730) GeV and 1440(1440) GeV. Combined analysis excludes masses of the RS Kaluza-Klein gravitons for couplings of 0.05 and 0.10 at 1450 GeV and 1780 GeV. The corresponding dimuon(dielectron) numbers are 1240(1300) GeV and 1640(1590) GeV.

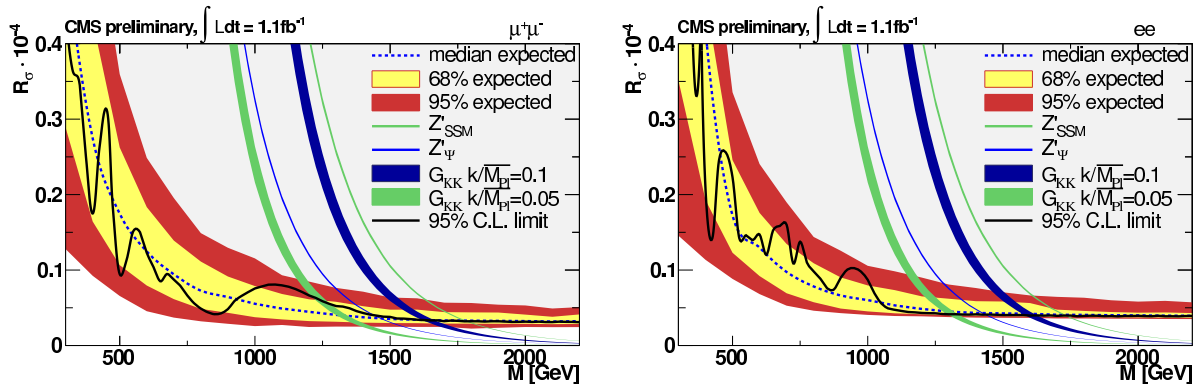


Figure 6: Exclusion limits on the dilepton resonance cross section times branching fraction relative to the Z-boson standard model production, dimuon channel (left) and dielectron channel (right).

We identify the most signal-like patterns in the data. They correspond to a dimuon resonance at 1080 GeV and a dielectron resonance at 950 GeV, with local significances of 1.7 and 2.2 standard deviations, respectively. Corrected for the “trials factor” (a consideration that a signal-like fluctuation can happen at an arbitrary mass value), the significances become 0.3 and 0.2 standard deviations, respectively. Combined analysis suggest a dilepton resonance-like signature at 970 GeV with local significance of 2.1 and significance corrected for the trials factor of 0.2 standard deviations. Figures 8 and 9 display the sampling distributions of the likelihood ratio test statistic (3) obtained from ensembles of background-only pseudoexperiments, used for estimating significances including the trials factor corrections, overlaid with the value from data.

10. Conclusion

The CMS Collaboration has searched for high-mass narrow resonances in the dilepton invariant mass spectra in the dimuon and the dielectron channels, using 1.1 fb^{-1} of integrated luminosity recorded by the CMS detector operating at the LHC proton-proton collider at CERN, with the center-of-mass energy of 7 TeV. The individual channel and combined spectra are consistent with the Standard Model expectations. The 95% C.L. upper limits have been set on the product of the new resonance production cross section and the corresponding branching fraction relative to the Standard Model Z boson production. Mass limits have been set on the resonances predicted by the SSM and Ψ $Z^{0'}$ models, and on the RS Kaluza-Klein gravitons for couplings of 0.05 and 0.1.

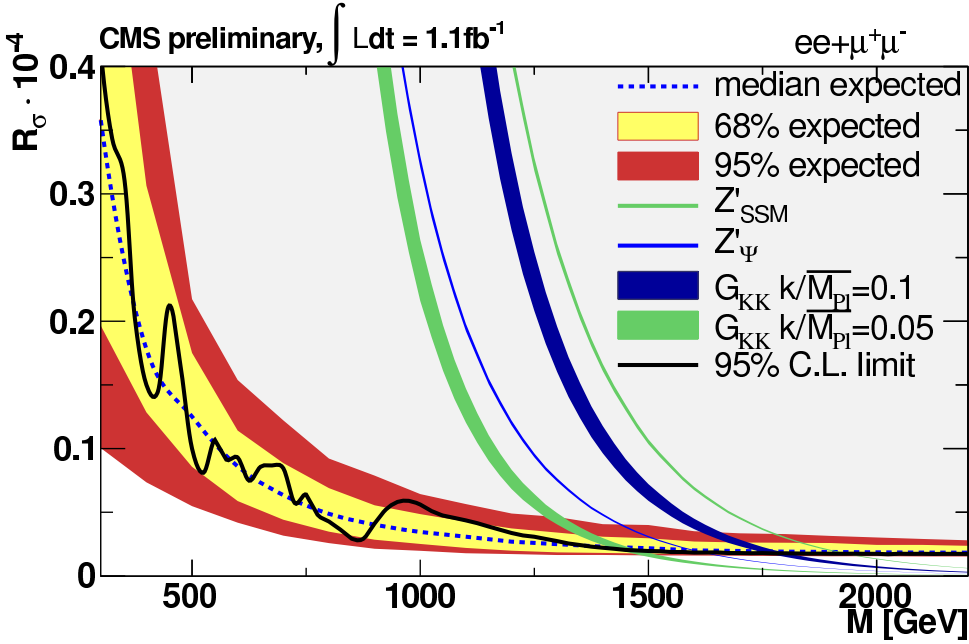


Figure 7: Combined dimuon and dielectron channel exclusion limits on the dilepton resonance cross section times branching fraction relative to the Z-boson standard model production.

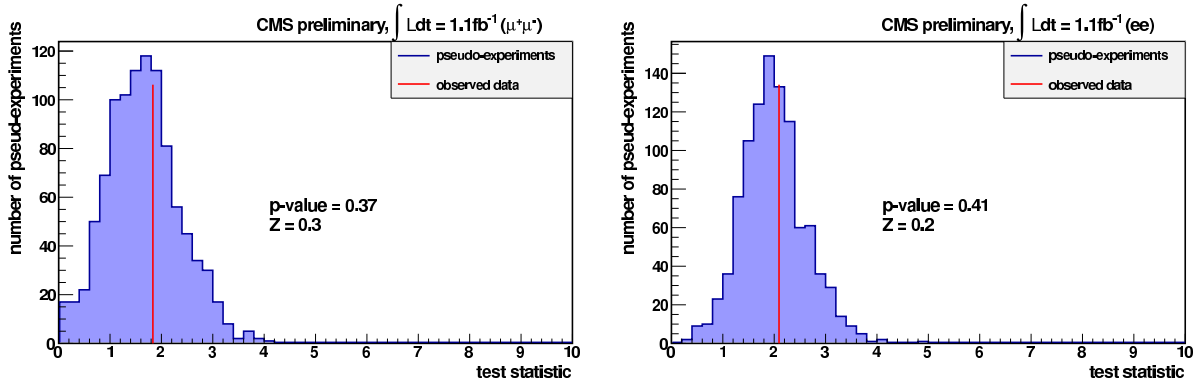


Figure 8: Significance in the dimuon channel (left) and in the dielectron channel (right). A histogram corresponds to an ensemble of background-only pseudoexperiments. The red line is a value observed in data. A plotted value corresponds to the most signal-like pattern in a dataset, in a fine scan of the spectrum over the allowed invariant mass values.

Acknowledgments

We wish to congratulate our colleagues in the CERN accelerator departments for the excellent performance of the LHC machine. We thank the technical and administrative staff at CERN and other CMS institutes, and acknowledge support from: FMSR (Austria); FNRS and FWO (Belgium); CNPq, CAPES, FAPERJ, and FAPESP (Brazil); MES (Bulgaria); CERN; CAS, MoST, and NSFC (China); COLCIENCIAS (Colombia); MSES (Croatia); RPF (Cyprus); Academy of Sciences and NICPB (Estonia); Academy of Finland, ME, and HIP (Finland); CEA and CNRS/IN2P3 (France); BMBF, DFG, and HGF (Germany); GSRT (Greece); OTKA and NKTH (Hungary); DAE and DST (India); IPM (Iran); SFI (Ireland); INFN (Italy); NRF and WCU (Korea); LAS (Lithuania); CINVESTAV, CONACYT, SEP, and UASLP-FAI (Mexico); PAEC (Pakistan); SCSR (Poland); FCT (Portugal); JINR (Armenia),

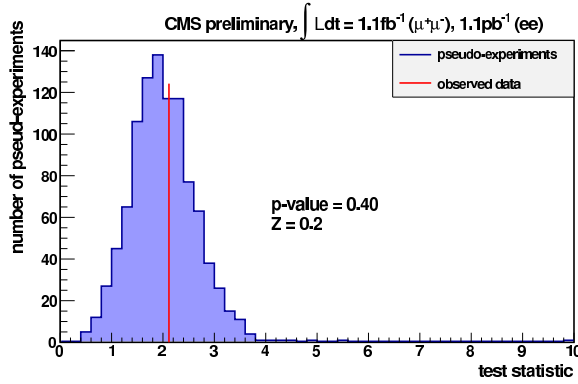


Figure 9: Combined significance in the two channels. A histogram corresponds to an ensemble of background-only pseudoexperiments. The red line is a value observed in data. A plotted value corresponds to the most signal-like pattern in a dataset, in a fine scan of the spectrum over the allowed invariant mass values.

Belarus, Georgia, Ukraine, Uzbekistan); MST and MAE (Russia); MSTD (Serbia); MICINN and CPAN (Spain); Swiss Funding Agencies (Switzerland); NSC (Taipei); TUBITAK and TAEK (Turkey); STFC (United Kingdom); DOE and NSF (USA).

References

- 1 A. Leike, The phenomenology of extra neutral gauge bosons, *Phys. Rept.* **317**, 143 (1999).
- 2 L. Randall, R. Sundrum, An alternative to compactification, *Phys. Rev. Lett.* **83**, 4690 (1999).
- 3 L. Randall, R. Sundrum, A large mass hierarchy from a small extra dimension, *Phys. Rev. Lett.* **83**, 3370 (1999).
- 4 V. M. Abazov, *et al.*, Search for Randall-Sundrum gravitons in the dielectron and diphoton final states with 5.4 fb^{-1} of data from $p\bar{p}$ collisions at $\sqrt{s} = 1.96 \text{ TeV}$, *Phys. Rev. Lett.* **104**, 241802 (2010).
- 5 V. M. Abazov, *et al.*, Search for a heavy neutral gauge boson in the dielectron channel with 5.4 fb^{-1} of $p\bar{p}$ collisions at $\sqrt{s} = 1.96 \text{ TeV}$, *Phys. Lett. B* **695**, 088 (2011).
- 6 T. Aaltonen, *et al.*, A search for high-mass resonances decaying to dimuons at CDF, *Phys. Rev. Lett.* **102**, 091805 (2009).
- 7 T. Aaltonen, *et al.*, Search for High-Mass e^+e^- Resonances in $p\bar{p}$ Collisions at $\sqrt{s} = 1.96 \text{ TeV}$, *Phys. Rev. Lett.* **102**, 031801 (2009).
- 8 J. Abdallah, *et al.*, Measurement and interpretation of fermion-pair production at LEP energies above the Z resonance, *Eur. Phys. J.* **C45**, 589 (2006).
- 9 S. Schael, *et al.*, Fermion pair production in e^+e^- collisions at 189-209-GeV and constraints on physics beyond the standard model, *Eur. Phys. J.* **C49**, 411 (2007).
- 10 G. Abbiendi, *et al.*, Tests of the standard model and constraints on new physics from measurements of fermion pair production at 189-GeV to 209-GeV at LEP, *Eur. Phys. J.* **C33**, 173 (2004).
- 11 P. Achard, *et al.*, Measurement of hadron and lepton-pair production in e^+e^- collisions at $s^{**}(1/2) = 192\text{-GeV} - 208\text{-GeV}$ at LEP, *Eur. Phys. J.* **C47**, 1 (2006).
- 12 R. Adolphi, *et al.*, The CMS experiment at the CERN LHC, *JINST* **3**, S08004 (2008).
- 13 T. Sjöstrand, S. Mrenna, P. Z. Skands, PYTHIA 6.4 Physics and Manual, *JHEP* **05**, 026 (2006).
- 14 F. Maltoni, T. Stelzer, MadEvent: Automatic event generation with MadGraph, *JHEP* **02**, 027 (2003).
- 15 S. Alioli, *et al.*, NLO vector-boson production matched with shower in POWHEG, *JHEP* **07**, 060 (2008).
- 16 P. Nason, A new method for combining NLO QCD with shower Monte Carlo algorithms, *JHEP* **11**, 040 (2004).
- 17 S. Frixione, P. Nason, C. Oleari, Matching NLO QCD computations with Parton Shower simulations: the POWHEG method, *JHEP* **11**, 070 (2007).
- 18 J. Pumplin, *et al.*, New generation of parton distributions with uncertainties from global QCD analysis, *JHEP* **07**, 012 (2002).

- 19 S. Agostinelli, *et al.*, GEANT4: A simulation toolkit, *Nucl. Instrum. Meth.* **A506**, 250 (2003).
- 20 Performance of muon identification in 2010 data, *CMS PAS MUO-10-004* (2011).
- 21 Electron reconstruction and identification at $\sqrt{s} = 7$ TeV, *CMS PAS EGM-10-004* (2010).
- 22 Measurements of Inclusive W and Z Cross Sections in pp collisions at $\sqrt{s} = 7$ TeV (2010). Submitted to *JHEP*.
- 23 CMS Collaboration, CMS technical design report, volume II: Physics performance, *J. Phys.* **G34**, 995 (2007).
- 24 K. Melnikov, F. Petriello, *Phys. Rev. D* **74**, (2006) 114017.
- 25 D. Stump, *et al.*, Inclusive jet production, parton distributions, and the search for new physics, *JHEP* **10**, 046 (2003).
- 26 K. Nakamura, *et al.*, Review of particle physics, *J. Phys.* **G37**, 075021 (2010).